

Coherently driven quantum metrology using a photonic de Broglie Sagnac interferometer

B. S. Ham

School of Electrical Engineering and Computer Science, Gwangju Institute of Science and Technology, 123

Chumdangwagi-ro, Buk-gu, Gwangju 61005, S. Korea

(Submitted on February 6, 2020)

A nonclassical feature of photonic de Broglie waves (PBW) has been studied over decades for fundamental quantum physics as well as potential applications of quantum metrology. Due to extremely low efficiency of higher-order entangled photon pair generations such as a NOON state, however, the implementation of PBW is extremely challenging. Here, a photonic de Broglie Sagnac interferometer is presented for a few orders of magnitude enhanced phase resolution, where the enhancement is due to coherently driven PBW in a cross-coupled double Mach-Zehnder interferometer. This method opens a door to coherence-quantum metrology such as lithography and sensing as well as inertial navigation and gyroscope in an optical regime.

Since the first demonstration in 1913 [1], the Sagnac interferometer (SI) has been implemented for optical [2] and matter-wave [3] interferometry and atomic spectroscopy [4]. The Sagnac interferometer has also been used for the detection of non-reciprocal properties such as magneto-optical Kerr effect in high-temperature superconductors better than $1 \mu\text{rad}/\sqrt{\text{Hz}}$ resolution [5]. The Sagnac effect of the rotation detection is caused by relativistic time difference Δt between counter-propagating lights in a closed loop, where $\Delta t = \frac{4A\Omega}{c^2}$, A is the area of the closed loop, and Ω is a rotation rate [6]. Due to small Δt , the SI has been limited to inertial navigation systems of aircrafts, rockets, drones, submarines, and space vehicles. Thus, in Sagnac applications, higher phase resolution is the utmost important parameter to achieve for both dynamic range ($\gg 360^\circ/\text{s}$) and sensitivity ($\ll \mu^\circ/\text{h}$). Although a fiber gyro system has been developed to overcome the size limitation in Δt [7], its phase resolution is too behind to be applied for inertial navigation systems due to lower sensitivity than a ring laser gyro system developed since 1970s [8]. Recently, such a fine phase resolution has also become an important issue in nanophotonic optical gyro platforms due to it's a weak signal to noise ratio, where controlling reciprocity is another issue [9,10].

To overcome the classical limit in sensitivity quantum nature of light has been studied for potential applications of quantum metrology [11-17]. As demonstrated in atomic interferometry [4], the advances in quantum measurement is in the photonic de Broglie wavelength (PBW), where entangled photons contribute to the enhanced phase resolution by the degree of entanglement [15]. Not only resolution but also sensitivity is reduced down below the standard quantum limit in PBW operating quantum metrology limited by Heisenberg limit [12,13]. However, the nonclassical light generation for quantum metrology is quite challenging, where the top record of entangled photon number N such as in a NOON state is just 18 at an extremely low efficiency [16]. Thus, quantum metrology has been practically halted in general.

Here, a completely different mechanism of SI is presented using coherence PBW [18] in a coherently driven cross-coupled double- (CCD) Mach-Zehnder interferometer (MZI): A photonic de Broglie Sagnac interferometer (PBSI). Recently, coherence PBW has been introduced for the fundamental quantum physics as well as its potential applications to quantum metrology to overcome both classical and quantum limits in phase resolution as well as sensitivity. The physics of coherence PBW is in the recursive quantum superposition in the CCD-MZI [18]. Each output from the unit cell of MZI has already been discussed for coherently driven nonclassical light generation such as anticorrelation or an entangled light [19]. With a sophisticated design of the recursive CCD-MZI, a quantum feature of PBW has also been represented [18]. Thus, the coherence PBW is equivalent to quantum PBW, where a specific phase relation between two coherent lights plays a key role for its nonclassical feature.

The fundamental limit of phase resolution in classical physics such as SI is given by the Rayleigh criterion governed by the wavelength λ_0 of light. In the quantum PBW, the classical limit is overcome by nonclassical feature of entangled photons or squeezed light, whose resolution is dependent upon the degree of nonclassicality [15-17]. In this case, the optical de Broglie wavelength λ_B is proportional to λ_0/N , where N represents the degree of entanglement such as N in a NOON state. For example, if $N=2$, the degree of nonclassicality is doubled compared with $N=1$ (classical limit). Thus, the phase resolution in PBW is enhanced by N . The degree of nonclassicality in the NOON state is represented by how many photons (N) are involved for the entanglement. Because achieving high N is extremely difficult, the implementation of quantum metrology is challenging [11-17]. On the contrary, achieving higher degree of nonclassicality in the present coherence PBW is quite easy and deterministic. For a potential application of coherence PBW, a PBSI is proposed, analyzed and discussed for a quantum version of SI, whose phase resolution is enhanced by at least a few orders of magnitude higher than the conventional one.

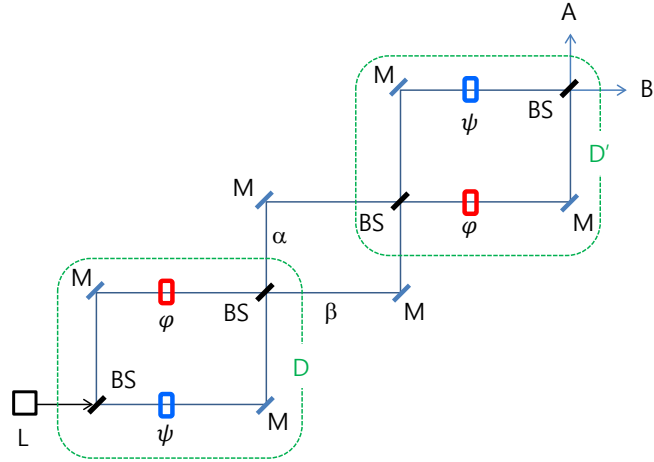


Fig. 1. A cross-coupled double-MZI for photonic de Broglie wavelength generation. L: laser, M: mirror, BS: beam splitter, φ/ψ : phase controller.

Figure 1 shows a basic building block of CCD-MZI for the PBSI using coherence PBW [17]. Instead of nonclassical light such as entangled photons [11-16], the input E_0 is a coherent light from a typical laser. The coherent light is not a few photon light but a phase coherent bright light. As already investigated on a beam splitter [19], the basic physics of coherence PBW is originated in quantum superposition between two paths of MZI, resulting in multi-order quantum superposition in a recursive MZI system [18]. Here, the basic unit of the recursive MZI is CCD-MZI to create the coherence PBW via doubly ordered quantum superposition. As discussed in ref. 18, the doubly ordered quantum superposition in CCD-MZI with one phase parameter is equivalent to $N=4$ in quantum PBW [16].

In Fig. 1, the output fields α and β in the first block D results in a nonclassical feature via anticorrelation if the relative phase is satisfied by $\Delta\phi = (\varphi - \psi) = \pm m\pi$, where $m=0,1,2,3\dots$. Then, the output field must be unidirectional either into α or β depending on m in $\Delta\phi$ [18]. Although E_0 is a coherent field, the output field (α or β) can be nonclassical via anticorrelation [19], and enters the second block D' resulting in the output A and B through the same mechanism for α or β . The quantum superposition in D' is thus the second order if the phase relation is opposite to that in D as shown in Fig. 1 [18]. This is the heart of coherence PBW. As demonstrated, PBW is an inherent quantum nature and cannot be obtained classically [15-17]. So does coherence PBW [18]. The CCD-MZI scheme has already been discussed for a quantum device to generate PBW in a completely different manner [18,19].

The followings are analytic expressions for the first MZI (block D) in Fig. 1 as functions of the independent phases φ and ψ :

$$\begin{bmatrix} \alpha \\ \beta \end{bmatrix} = [BS][\Theta][BS] \begin{bmatrix} E_0 \\ 0 \end{bmatrix},$$

$$= \frac{1}{2} e^{i\psi} \begin{bmatrix} (1 - e^{i(\varphi-\psi)}) & i(1 + e^{i(\varphi-\psi)}) \\ i(1 + e^{i(\varphi-\psi)}) & -(1 - e^{i(\varphi-\psi)}) \end{bmatrix} \begin{bmatrix} E_0 \\ 0 \end{bmatrix}, \quad (1)$$

where $[BS]$ and $[\Theta]$ are $\frac{1}{\sqrt{2}} \begin{bmatrix} 1 & i \\ i & 1 \end{bmatrix}$ and $\begin{bmatrix} e^{i\psi} & 0 \\ 0 & e^{i\varphi} \end{bmatrix}$, respectively (see the Supplementary Material). Thus, the light intensity of α and β are, respectively:

$$I_\alpha = \frac{I_0}{2} [1 - \cos(\varphi - \psi)] \quad (= I_0 \sin^2[(\varphi - \psi)/2]), \quad (2-1)$$

$$I_\beta = \frac{I_0}{2} [1 + \cos(\varphi - \psi)] \quad (= I_0 \cos^2[(\varphi - \psi)/2]), \quad (2-2)$$

where I_0 is the intensity of E_0 . Compared with conventional one-phase-based MZI [18], whose modulation period is 2π , equations (2-1) and (2-2) can result in a double modulation period if an antiphase relation is satisfied for $\varphi = -\psi$.

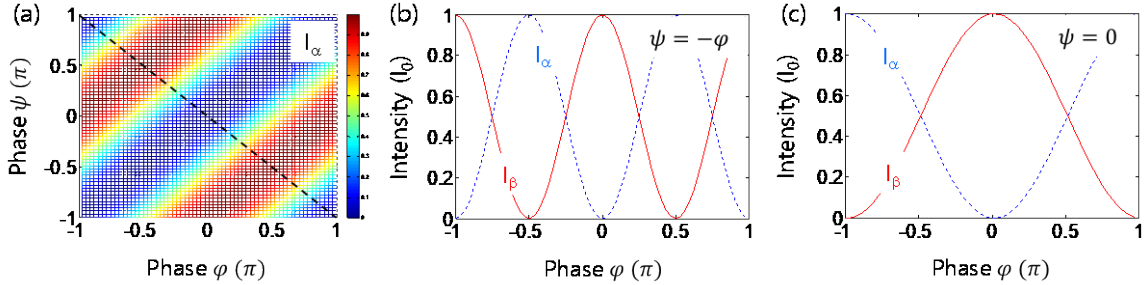


Fig. 2. Numerical calculations for the first MZI outputs in Fig. 1. (a) I_α of equation (2-1). (b) For $\psi = -\varphi$. (c) For $\psi = 0$. For I_β of equation (2-1), see the Supplementary Material.

In Fig. 2, the first MZI outputs I_α and I_β are numerically calculated using equations (2-1) and (2-2). As shown in Fig. 2(a), the modulation period depends on the relative phase relation between φ and ψ , where it is maximized if an antiphase ($\psi = -\varphi$) relation is satisfied along the dashed line as shown in Fig. 2(b). In Fig. 2(b), the anticorrelation $g^{(2)} = 0$ is obtained at $\varphi = \pm m\pi/2$. This $\pi/2$ modulation period is the same as the quantum PBW with $N=4$ [16]. Figure 2(c) shows a reference of a classical limit in a typical MZI if $\psi = 0$, where it represents for the Rayleigh criterion or the diffraction limit of $\lambda_0/2$, and λ_0 is the wavelength of E_0 . According to the classical physics, the phase/spatial resolution is strongly limited by the wavelength of light. Thus, the condition of antiphase in Fig. 1 results in the $\lambda_0/4$ ($\pi/2$) in spectroscopy beyond the classical limit as shown in Fig. 2(b). Here, the antiphase relation is automatically satisfied in SI due to the Sagnac effect: $\Delta\phi = \phi_{ccw} - \phi_{cw} = 2\varphi$ (see also Figs. 2(b) and 3(b)) [1-10].

In the CCD-MZI of Fig. 1, the matrix representation for the final outputs A and B is as follows (see the Supplementary Material):

$$\begin{bmatrix} A \\ B \end{bmatrix} = [BS][\Theta'][BS] \begin{bmatrix} \alpha \\ \beta \end{bmatrix}, \\ = e^{i(\varphi+\psi)} \begin{bmatrix} \cos(\varphi - \psi) & \sin(\varphi - \psi) \\ -\sin(\varphi - \psi) & \cos(\varphi - \psi) \end{bmatrix} \begin{bmatrix} E_0 \\ 0 \end{bmatrix}, \quad (3)$$

where $[\Theta'] = \begin{bmatrix} e^{i\varphi} & 0 \\ 0 & e^{i\psi} \end{bmatrix}$. Thus, intensities I_A and I_B of A and B are, respectively:

$$I_A = I_0 \cos^2(\varphi - \psi), \quad (4-1)$$

$$I_B = I_0 \sin^2(\varphi - \psi). \quad (4-2)$$

As numerically demonstrated in Fig. 3(a), the modulation frequency of I_A with respect to φ is twice higher than that in Fig. 2(a). The maximum modulation frequency appears at the antiphase relation of $\psi = -\varphi$ as shown in Fig. 3(b). The lowest modulation frequency (or resolution) is achieved at $\psi = 0$ as shown in Fig. 3(c), which is equivalent to Fig. 2(b), the four-photon quantum PBW [16]. Thus, the CCD-MZI of Fig. 3(a) is

equivalent to $N=8$ in quantum PBW [17]. From Fig. 3, an n -folded modulation frequency can be obtained in a recursive configuration based on CCD-MZI of Fig. 1. Such a result has already been discussed in a chain of a single-phase MZI scheme for individual coherence PBW [18]. Here, a collective version of coherence PBW is presented for the PBSI.

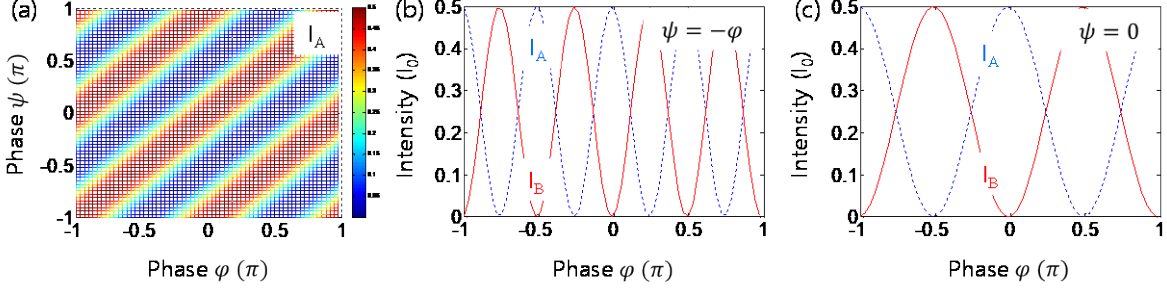


Fig. 3. Numerical calculations for the second MZI outputs in Fig. 1. (a) I_A for equation (4-1). (b) For $\psi = -\varphi$. (c) For $\psi = 0$. For I_B , see the [Supplementary Material](#).

For the recursive configuration using CCD-MZI of Fig. 1, a cavity PBSI of Fig. 4(a) is proposed for the realization of the present coherence PBW, where the antiphase condition of $\psi = -\varphi$ is automatically satisfied in SI. The cavity PBSI of Fig. 4(a) becomes an intrinsic quantum device satisfying anticorrelation if the antiphase condition is met for all ordered coherence PBWs. Here, the maximum order of PBWs is determined by the optical *Finesse* \mathcal{F} : $\mathcal{F} = \frac{\pi\eta}{1-\eta^2}$. Due to the reflection coefficient η on the cavity mirror C in Fig. 4(a), the ordered amplitudes of PBW are gradually reduced as the order n increases. Here, n is the repetition number of CCD-MZI in the cavity of Fig. 4(a) and determined by \mathcal{F} .

The n^{th} order of PBW inside the cavity in Fig. 4(a) is represented as follows (see the [Supplementary Material](#)):

$$(E_A)^n = (-1)^n \eta^{2(n-1)} E_0 \cos(2n\varphi), \quad (5-1)$$

$$(E_B)^n = (-1)^{n+1} \eta^{2(n-1)} E_0 \sin(2n\varphi). \quad (5-2)$$

As driven in equations (5-1) and (5-2), each even ordered field is perfectly cancelled out by each odd ordered one due to the prefactor of $(-1)^n$ or $(-1)^{n+1}$, respectively, if $2n\varphi = \pm 2m\pi$ is met. Thus, the sum of all n -ordered amplitudes in each field of equations (5-1) and (5-2) becomes zero at $\varphi \rightarrow \varphi_{mn}^d = \pm m\pi/n$, where the sinusoidal functions has a sign flip for n (see the colored curves in Fig. 4(b) for a fixed m). If $n \gg 1$, $(E_A)^n$ locates nearly everywhere regularly in the phase axis due to n^{-1} factor in φ_{mn}^d , where each $(E_A)^{n+1}$ has a sign flip with respect to $(E_A)^n$, resulting in a complete destructive interference for all n in the phase axis, except for $\varphi = \pm m\pi/2$ (discussed below).

On the contrary, for $2n\varphi = \pm(2m+1)\pi$, equations (5-1) and (5-2), however, result in a constructive interference due to the sign flip in each sinusoidal function whenever φ is doubled for $n \geq 2$ exactly compensating the prefactor-induced sign flip (see the arrows in Fig. 4(b)). Thus, the phase condition for the constructive interference occurs at $\varphi \rightarrow \varphi_{mn}^c = \pm \left(\frac{(2m+1)\pi}{2}\right) \frac{1}{n}$ (discussed below).

For simplicity, let's set $m=0$ in equation (5-1) and discuss for the constructive interference. For the first order $n=1$, $(E_A)^{n=1} = (-1)^1 \eta^0 E_0 = -E_0$ at $\varphi_{01}^c = \pm \frac{\pi}{2}$ (see the blue curve in Fig. 4(b)). Remember that the CCD-MZI has a $\frac{\pi}{2}$ modulation period in intensity in Fig. 2, resulting in π modulation in amplitude. Thus, there is a sign flip whenever it is evenly multiplied. For the second order $n=2$, $(E_A)^{n=2} = (-1)^2 \eta^2 E_0 = \eta^2 E_0$ at $\varphi_{02}^c = \pm \frac{\pi}{4}$. Thus, $(E_A)^{n=2}$ becomes flipped over to $-\eta^2 E_0$ at $\varphi = \pm \frac{\pi}{2}$, i.e., $\varphi = 2\varphi_{12}^c$. For the third order, $n=3$, $(E_A)^{n=3} = (-1)^3 \eta^4 E_0 = -\eta^4 E_0$, at $\varphi_{13} = \pm \frac{\pi}{6}$. Thus, $(E_A)^{n=3}$ has no flip at $\varphi = \pm \frac{\pi}{2}$ due to an odd multiple, resulting in $-\eta^3 E_0$ at $\varphi = 3\varphi_{13}^c$ (see the green curve in Fig. 4(b)). For the forth order, $n=4$, $(E_A)^{n=4} = (-1)^4 \eta^6 E_0 = \eta^6 E_0$ is satisfied at $\varphi_{13} = \pm \frac{\pi}{8}$. Thus, $(E_A)^{n=4}$ is flipped over and becomes $-\eta^6 E_0$

at $\varphi = \pm \frac{\pi}{2}$, i.e., $\varphi = 4\varphi_{13}^c$. As a result, all n-ordered components in equation (5-1) results in the constructive interference at $\varphi_{mn}^c = \pm \left(\frac{(2m+1)\pi}{2}\right) \frac{1}{n}$, and the output field A from the cavity PBSI in Fig. 4(a) becomes $E_A = -E_0 \sum_{n=1} \eta^{2(n-1)}$ at $\varphi = \pm \left(\frac{(2m+1)\pi}{2}\right)$: For E_B , see [the Supplementary Material](#).

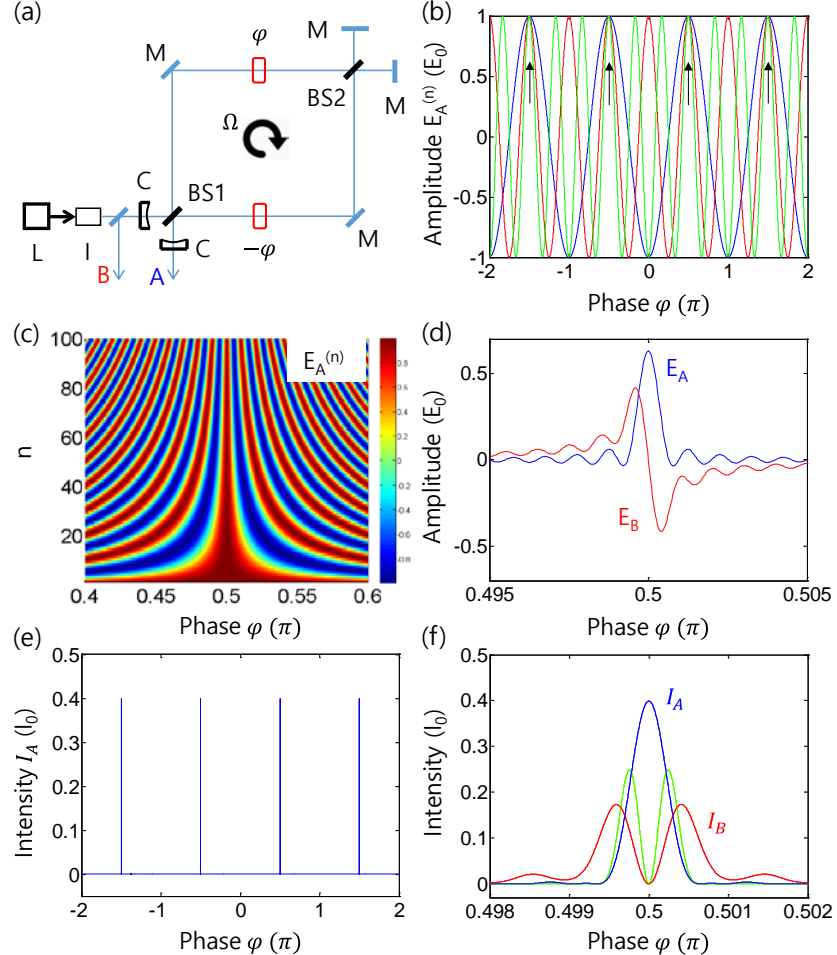


Figure 4. A Cavity photonic de Broglie Sagnac interferometer and its numerical calculations. (a) A schematic of cavity PBSI based on the present coherence PBW. (b)-(f) Numerical calculations for (a). (b) Each ordered field (E_A) for the output A in (a): Blue, $n=1$; Red, $n=2$; Green, $n=3$; n represents number of light circulation in (a). The arrows indicate common phase bases resulting in constructive interference. (c) All ordered components of E_A . (d) Amplitude average of (c). E_B^S is for the output B. (e) Output intensity for I_A^S . (f) Details of (e): The green dotted curve is the intensity correlation of I_A^S and I_B^S indicating $g^{(2)}$. L: laser, I: optical isolator, C: cavity mirror, M: mirror, BS: 50/50 beam splitter. For numerical calculations, $n=1,000$ and $\eta=0.999$, where η is the reflection coefficient of C. For E_B and I_B^S , see [the Supplementary Material](#).

Figure 4(c) shows numerical calculations for the ordered components with $n=100$ using equation (5-1) as a function of phase φ , where $\psi = -\varphi$ (antiphase). As analyzed above, $(E_A)^n$ in equation (5-1) shows the constructive interference at $\varphi = \pi/2$ proving the above analysis: see [the Supplementary Material](#) for equation (5-2). More importantly, the phases for all ordered components are fully in phase at $\varphi = \pi/2$, where the spectral width is determined by the last ordered one (see [the Supplementary Material](#)). Figure 4(d) shows the amplitude sum E_A and E_B as a function of φ for $n=1,000$, demonstrating not only the constructive interference but also in phase relation at $\varphi = \pi/2$. Here, the loss is only due to η on the cavity mirror C. Thus, the amplitude sum of each output A and B in the cavity PBSI results in ultrasharp spectral lines whenever

$\varphi = \pm \left(\frac{(2m+1)\pi}{2} \right)$ is satisfied, otherwise becomes zero due to destructive interference. The spectroscopic sharpness is inversely proportional to the number of repetition n of CCD-MZI for PBSI (discussed in Figs. 4(e) and (f)).

The intensity of output fields A and B in Fig. 4(a) is calculated from the sum fields E_A and E_B , respectively, as shown in Fig. 4(e):

$$I_A = E_A E_A^*, \quad (6-1)$$

$$I_B = E_B E_B^*, \quad (6-2)$$

where $E_A = \sum_n (E_A)^n$ and $E_B = \sum_n (E_B)^n$. As analyzed above in Figs. 4(b)~(d) and numerically calculated in Figs. 4(e) and (f), the intensity (I_A and I_B) of each output field A and B results in ultranarrow discrete spectral lines at $\varphi = \pm \left(\frac{(2m+1)\pi}{2} \right)$, whose phase resolution is of course ultraenhanced due to n : see [the Supplementary Material](#) for I_B . Unlike the classical resolution δf_C limited by $\lambda_0/4$ ($\pi/2$) on a Sagnac interferometer (see Fig. 2(b)), the present cavity PBSI of Fig. 4(f) results in $\delta f_{PBSI} = \frac{\delta f_C}{2n}$. Regarding I_B of equation (6-2), the sine function-induced asymmetric feature in E_B (see red curve in Fig. 4(d)), however, results in double spectroscopic lines (see red curve in Fig. 4(f)). So does the intensity correlation $g^{(2)}$ between the outputs I_A and I_B (see the green dotted curve).

Thus, for $n=1,000$ with $\eta = 0.999$ in Fig. 4, the phase resolution enhancement factor in the cavity PBSI reaches at 2,000 as demonstrated analytically and numerically in Figs. 4(d) ~ (f). Compared with all existing (classical) SI techniques, the present cavity PBSI based on recursive CCD-MZI of Fig. 1(a) offers unprecedented result in a few orders of magnitude better than the conventional one. The physics of high resolution in Fig. 4 is due to new understanding of anticorrelation in MZI in a recursive configuration and its smart application to the cavity PBSI. The system, preparation, and measurement techniques are all classical and simple. The end mirror with 99.9% reflection coefficient ($\eta = 0.999$) is commercially available. Even with low reflectance such as 90%, the present CBS works fine for the spectral linenarrowing far beyond the conventional limit without deterioration in resolution (see [the Supplementary Material](#)). Even the use of intensity correlation in Fig. 4(f) gives a few factors more enhanced resolution. In addition, the potential well of $g^{(2)}$ in Fig. 4(f) may be applied for signal locking in sub-Hz laser systems. In a short summary, our understanding on quantum mechanics is now expanded from the particle nature of individual photons to the wave nature of collective photons via coherence PBW for the present cavity PBSI.

In conclusion, the coherence version of photonic de Broglie waves (PBW) in a cross-coupled double Mach-Zehnder interferometer (CCD-MZI) was presented for fundamental physics and its potential applications to Sagnac interferometer (SI). The coherence PBW was analyzed and compared with the conventional quantum PBW, whose phase resolution enhancement is due to the ordered quantum superposition of MZI in a recursive configuration. Therefore, this work intrigues quantum physics community to think about the origin of nonclassicality and quantum metrology in terms of coherence rather than just photon number. The coherently driven nonclassical feature of PBW results in enhanced phase resolution in a cavity photonic de Broglie Sagnac interferometer (PBSI). For the cavity PBSI, unprecedented spectroscopic resolution was achieved in a few orders of magnitude better than the conventional SI. The enhancement factor in the phase resolution is due to constructive interference among ordered components in PBSI, where the *Finesse*-determined effective order determines its phase resolution. The design of the cavity PBSI is pretty simple but smart offering unprecedented achievement in the phase resolution far beyond classical limit. The cavity PBSI may open a door to a new realm of coherence-quantum metrology in the fields of gyroscope, inertial navigation, optical clocks [20], lithography, and sensing. Owing to the huge enhancement factor in the phase resolution, the cavity PBSI can also be applied to a micro-Sagnac interferometer applicable to drones and robots [9].

Reference

1. Sagnac, G. *C. R. Acad. Sci.* **95**, 708-710 (1913); G. Sagnac, *C. R. Acad. Sci.* **95**, 1410-1413 (1913).

2. Shahriar, M. S., Pati, G. S., Tripathi, R., Gopal, V., Messall, M. & Salit, K. Ultrahigh enhancement in absolute and relative rotation sensing using fast and slow light. *Phys. Rev. A* **75**, 053807 (2007).
3. Barrett, B. et al. TheSagnac effect: 20 years of development in matter-wave interferometry. *C. R. Physique* **15**, 875-883 (2014).
4. Bustavson, T. L., Landragin, A. & Kasevich, M. A. Rotation sensing with a dual atom-interferometer Sagnac gyroscope. *Class. Quantum Grav.* **17**, 2385-2398 (2000).
5. Post, E. J. Sagnac effect. *Rev. Mod. Phys.* **39**, 475 (1967).
6. Fried, A., Fejer, M. & Kapitulnik, A. A scanning, all-fiber Sagnac interferometer for high resolution magneto-optic measurement at 820 nm. *Review of Sci. Instrument.* **85**, 103707 (2014)
7. Geiger, R. et al. Detecting inertial effects with airborne matter-wave interferometry. *Nat. Communi.* **2**, 474 (2011).
8. Chow, W. W. et al. The ring laser gyro. *Rev. Mod. Phys.* **57**, 61-104 (1985).
9. Khial, P. P., White, A. D. & Hajimiri, A. Nanophotonic optical gyroscope with reciprocal sensitivity enhancement. *Nature Photon.* **12**, 671-675 (2018).
10. Li, J., Suh, M. G. & Vahala, K. Microresonator Brillouin gyroscope. *Optica* **4**, 346-348 (2017).
11. Pezze, L. et al., Quantum metrology with nonclassical states of atomic ensemble. *Rev. Mod. Phys.* **90**, 035005 (2018).
12. Hosten, O., engelsen N. J., Krishnakumar, R. & Kasevich, M. A. Measurement noise 100 times lower than the quantum-projection limit using entangled atoms. *Nature* **529**, 505-508 (2016).
13. Giovannetti, V., Lloyd, S. & Maccone, L. Advances in quantum metrology. *Nature Photon.* **5**, 222-229 (2011).
14. Kira, M., Koch, S. W., Smith, R. P., Hunter, A. E. & Cundiff, S. T. Quantum spectroscopy with Schrodinger-cat states. *Nature Phys.* **7**, 799-804 (2011).
15. Jacobson, J., Gjörk, G., Chung, I. & Yamamoto, Y. Photonic de Broglie waves. *Phys. Rev. Lett.* **74**, 4835-4838 (1995).
16. Walther, P., Pan, J.-W., Aspelmeyer, M., Ursin, R., Gasparon, S. & Zeillinger, A. De Broglie wavelength of a non-local four-photon state. *Nature* **429**, 158-161 (2004).
17. Wang, X.-L. et al., 18-qubit entanglement with six photons' three degree of freedom. *Phys. Rev. Lett.* **120**, 260502 (2018).
18. Ham, B. S. Deterministic control of photonic de Broglie waves using coherence optics: Coherence de Broglie waves. arXiv:2001.06913v4 (2020).
19. Ham, B. S. the origin of anticorrelation for photon bunching on a beam splitter. arXiv:1911.07174v2 (2019).
20. Ludlow, A. D., Boyd, M. M., Ye, J., Peik, E. & Schmidt, P. O. Optical atomic clock. *Rev. Mod. Phys.* **87**, 637-701 (2015).